

## New Methods for Investigating Superconductivity at Very High Pressures

VIKTOR V. STRUZHKIN<sup>(1)</sup>, YURI A. TIMOFEEV<sup>(2)</sup>, EUGENE GREGORYANZ<sup>(1)</sup>, RUSSELL J. HEMLEY<sup>(1)</sup>, HO-KWANG MAO<sup>(1)</sup>

<sup>(1)</sup> *Geophysical Laboratory and Center for High Pressure Research, Carnegie Institution of Washington, 5251 Broad Branch Rd, N. W., Washington D.C. 20015*

<sup>(2)</sup> *Institute for High Pressure Physics, Russian Academy of Sciences, Troitsk 142 092, Russia*

### 1. – Introduction

As a result of rapid developments in diamond-cell techniques, a broad range of studies of the physical and chemical properties of solids can be now conducted *in situ* to megabar pressures (i.e.,  $> 100$  GPa). The highest superconducting  $T_c$  has been achieved by application of pressure of  $\sim 30$  GPa on  $\text{HgBa}_2\text{Ca}_2\text{Cu}_3\text{O}_{8+\delta}$  giving critical superconducting temperature of 164 K [3]. The same material has a record  $T_c=133$  K at ambient pressure. It took almost 30 years after the theory of superconductivity by Bardeen, Cooper and Schrieffer (BCS) in 1957 [4], and more than 75 years after discovery of the first superconductor by Kamerlingh Onnes in 1911 [5] (Hg, with a  $T_c=4.15$  K) to produce the first material that was superconducting above the boiling point of nitrogen (77.3 K):  $\text{YBa}_2\text{Cu}_3\text{O}_{7-x}$  with  $T_c=91(2)$  K [6]. Notably, it was a consideration of the effect of pressure on the 40 K La-cuprates [7] that guided experiments leading to the 90 K  $\text{YBa}_2\text{Cu}_3\text{O}_{7-x}$  superconductor [6]. Such applications of pressure allow to tune over a broad range electronic, magnetic, structural and vibrational properties of solids [1, 2]. Earlier techniques have been adapted to very small sample volumes (typical sample size in high pressure experiment is about  $100 \times 100 \times 20 \mu\text{m}^3$  at 30 GPa) to measure superconducting transitions inductively (by using magnetic susceptibility methods) or by direct conductivity methods at high pressures. The samples must be further reduced in size when a pressure medium is used (which is mandatory for many applications), and also for very high pressure experiments to above 100 GPa. To handle these demanding tasks new methods have been developed to measure superconducting transitions by utilizing Meissner effect in very small samples. We will present here in-depth discussion of a relatively new double-frequency modulation technique. The technique was used in measurements of  $T_c$  in sulfur to 230 GPa without pressure medium [8], and in recent measurements of superconductivity in  $\text{MgB}_2$  to 44 GPa in He pressure media [9]. The direct conductivity methods have recently been extended to pressures of 250 GPa [10].

The chapter is organized as follows. We start with an overview of magnetic techniques in Section 2. We then give a detailed description of double-frequency modulation technique. In Section 4 we discuss the pressure effects on superconductivity in simple s-p metals. The  $T_c(P)$  in the chalcogens is given in Section 5. In Section 6 we present pressure data for the recently discovered high-temperature superconductor  $\text{MgB}_2$ .

## 2. – Overview of existing techniques

One of the very first techniques for measuring  $T_c(P)$  in superconductors is well described in a review by Klotz, Schilling, and Müller [11]. This is a single-frequency standard technique often used at ambient pressure and adapted for diamond anvil cell experiment. The technique is capable of detecting signals from the samples as small as 80  $\mu\text{m}$  in diameter. Similar technique was developed by Tissen and used in measurements of  $T_c$  in La to 50 GPa [12].

Several other techniques have been developed in recent years [13, 14, 15] to overcome the problem of the background signal in single-frequency technique. The most notable techniques are the third-harmonic method [14], and the vibrating magnetometer technique [15]. Both techniques are capable of measuring signal from very small samples; however, the smallest possible sample size was not estimated in the original publications [15, 14]. The vibrating magnetometer technique has been used to detect superconductivity in vanadium to 120 GPa where  $T_c=17.2$  K [16].

The method presented here was introduced by Timofeev [13]. We have addressed the techniques for measurements of superconducting critical temperatures and Curie temperatures in ferromagnets recently [17, 18]. The technique has been used to the highest pressure of 230 GPa [8], and keeps the record for high-pressure magnetic susceptibility measurements of superconducting  $T_c$ .

The highest reported pressure of 250 GPa for superconductivity measurements was reached recently in experiment on boron [10] by electrical conductivity technique. We refer the reader to original papers and reviews on the progress in investigation of transitions from insulating to metallic states and  $T_c$  measurements in high-pressure metals by resistivity methods [10, 19, 20]. Here we will focus on measurements of superconducting transitions by magnetic susceptibility techniques in diamond anvil cell.

## 3. – Double-frequency modulation method

**3.1. Overview of the technique.** – We begin with a discussion of problems that arise when measuring magnetic properties of a small superconducting sample in a system consisting of signal and compensating (secondary) and exciting (primary) inductance coils located in the vicinity of the sample (Fig.1). The exciting coil (1) creates an alternating magnetic field which produces electromotive forces in both the signal (3) and compensating (2) coils. These coils are included in the electrical circuit in such a manner that their electromotive forces act in opposite directions and nearly compensate for each other. The difference between the two electromotive forces determines the background signal with magnitude depending on several factors. The most significant are (a) differences in the geometric parameters of the signal and compensating coils and their unavoidable asymmetric disposition inside the exciting coil, and (b) the proximity of the system of coils to metal parts of the high-pressure chamber (not shown in the figure), which distort the uniform distribution of magnetic flux passing through signal and compensating coils due to geometric asymmetry and electrical conductivity.

A modulation technique can be applied to detect the superconducting critical temperature due to the fact that one can “virtually” remove the superconducting sample from the high pressure cell by applying an external magnetic field that destroys superconductivity in the sample. The technique is based on the fact that the magnetic susceptibility of superconducting materials depends on the external magnetic field enclosed in the volume of the sample. When the magnetic field is high enough to quench the superconductivity,

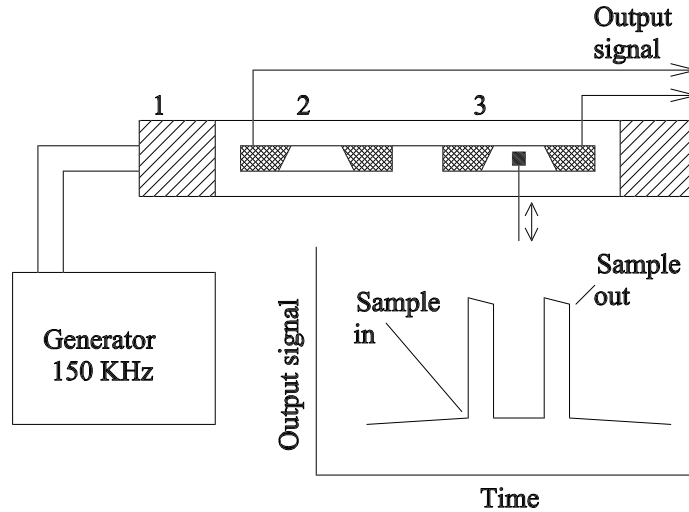


Fig. 1. – Schematic representation of the background subtraction principle in magnetic susceptibility measurements: 1 - primary coil; 2 - secondary compensating coil; 3 - secondary signal coil. Removal of the sample from the signal coil produces measurable changes in the total output signal.

the Meissner effect is suppressed and the magnetic field penetrates the sample volume. (This happens at the critical magnetic field  $H_c$ ). In contrast, the susceptibility of the metallic parts of the high-pressure cell (diamagnetic and paramagnetic) is essentially independent of the external field. Thus, insertion of the high-pressure cell containing the sample in an external magnetic field exceeding the critical value changes the part of the signal produced by the sample, while the background remains practically constant. This fact allows the separation of the signal arising from the sample from that of the background. We apply the low-frequency ( $f = 22$  Hz) magnetic field with an amplitude up to several dozen Oersted, which causes the destruction of the superconducting state near the superconducting transition. This in turn leads to a change in the magnetic susceptibility of the sample from  $-1$  up to  $0$  twice in a given period, and produces a modulation of the signal amplitude in the receiving coils at a frequency  $2f$ . The subsequently amplified signal from the lock-in amplifier is then recorded as a function of temperature on the computer. The critical superconducting temperature  $T_c$  is then identified as the point where the signal goes to zero due to the disappearance of the diamagnetic signal at  $T_c$ . Fig. 2 shows the outline of the system of coils and relevant electronics for detecting the double-frequency  $2f$  modulated signal.

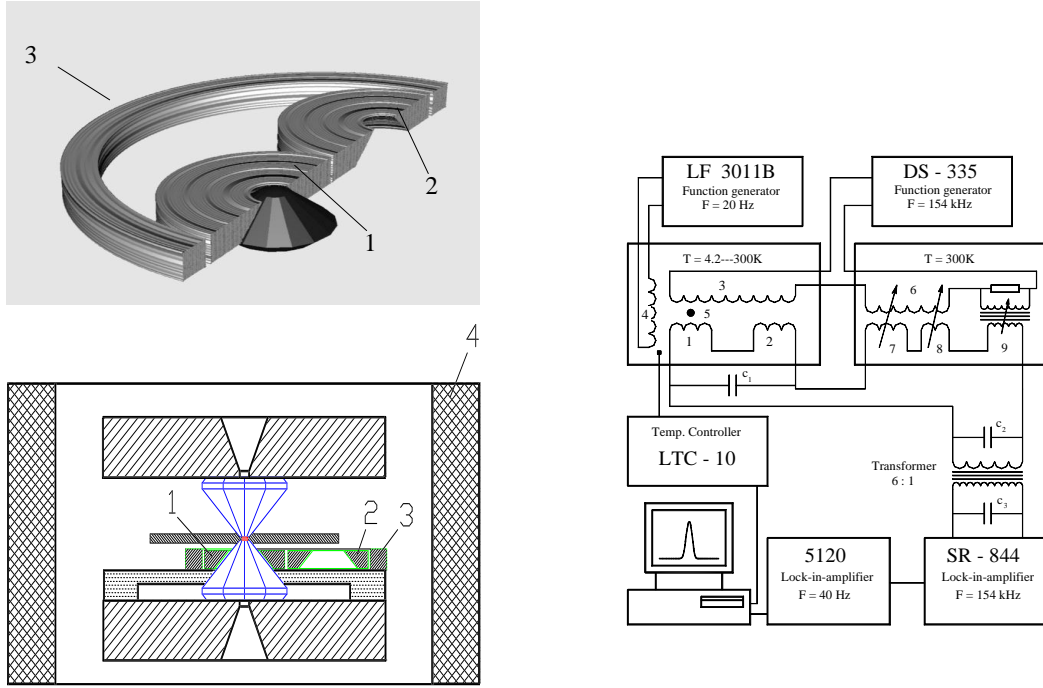


Fig. 2. – Schematic of the double-frequency modulation setup. Coil 4 is used to apply low frequency magnetic field to modulate the amplitude response from the high-frequency pick-up coil 2 due to the superconducting sample. The setup includes two signal generators and two lock-in amplifiers, operating at low (20-40Hz) and high (155KHz) frequencies. Details are presented elsewhere [18].

**3.2. Signal shape.** – The dependence of the signal on temperature for the outlined double-frequency modulation technique can be estimated using the Hao-Clemm model for reversible magnetization in type II superconductor [21]. Hao-Clemm theory has been highly successful in describing the magnetization curves of high- $T_c$  superconductors, and is valid in the temperature and field region where magnetization is thermodynamically reversible and fluctuation effects are not important. Figure 3 shows the magnetization curves for type I and type II superconductors. We illustrate the time dependence of the magnetic field at the sample position in Fig. 4. When the temperature increases and approaches  $T_c$ , the critical magnetic field  $H_{c1}$  decreases (almost linearly close to  $T_c$ ), reaching zero at  $T_c$ . Using magnetization curves for type II superconductor we have calculated numerically the signal at the second harmonic of the low-frequency magnetic field, which is shown in Fig. 5. The signal starts developing when  $H_{c1}$  is equal to the amplitude of the low-frequency magnetic field (temperature  $T_1$ , Fig. 4) and reaches its maximum at temperature  $T_{max}$ , which is determined by the actual values of the parameters involved. The signal drops to zero at  $T_c$ . We assumed in the calculation that  $H_{c1}$  is a linear function of  $(T_c - T)$  close to  $T_c$ . The numerically calculated signal shape does not depend significantly on the value of the Ginzburg-Landau parameter and is shown in

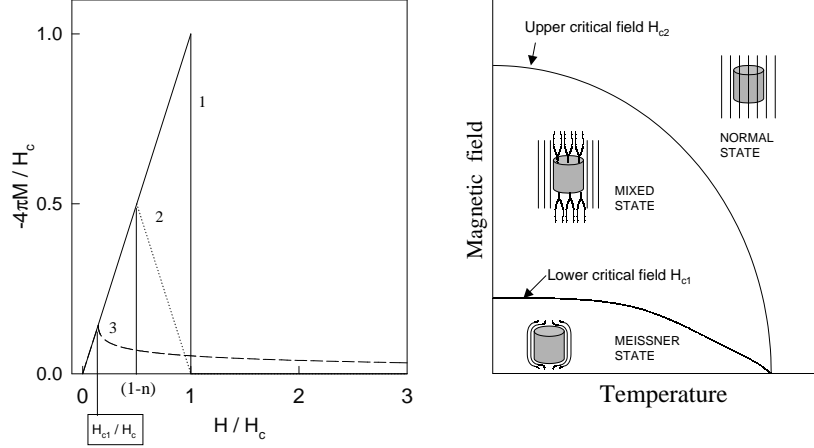


Fig. 3. – Magnetization curves for type I and type II superconductors. 1 - ideal type I superconductor; 2 - type I superconductor, with demagnetization factor taken into account; 3 - magnetization curve for type II superconductor. Right panel shows schematically where Meissner state, mixed state, and normal state are located in H-T space for type II superconductor. It shows also that  $H_{c1}$  is almost linear close to  $T_c$ .

Fig. 5. The signal shapes calculated for different magnetization curves are close to the signal shape observed in experiments on  $\text{YBa}_2\text{Cu}_3\text{O}_{7-x}$  in He pressure medium (Fig. 6). Our assumptions of reversible magnetization are supported by reported magnetization measurements in  $\text{YBa}_2\text{Cu}_3\text{O}_{7-x}$  between 80 and 90 K [22]. However, more realistic calculations should take into account the irreversibility effect on the magnetization curves near  $T_c$ , similar to calculations performed in Ref. [23] for the signal shape at the third harmonic of the excitation frequency.

**3.3. Sensitivity.** – The crucial parameter for such a system is its sensitivity. We give below a simple estimate of the sensitivity based on classical electrodynamics. The sample is very small and acts as a magnetic dipole with a magnetic moment (in SI units)  $M = V_s \chi B / \mu_0$  (where  $V_s$  is the sample volume,  $\chi$  is magnetic susceptibility,  $B$  is magnetic induction, produced by excitation coils, and  $\mu_0 = 4\pi \cdot 10^{-7}$  H/m is the magnetic permeability of a vacuum). The EMF induced by the sample on the detection coils is

$$(1) \quad \varepsilon = 2\pi f \frac{n}{D} V_s \chi B,$$

where  $f$  is the frequency of the exciting field,  $n$  is number of turns, and  $D$  is a diame-

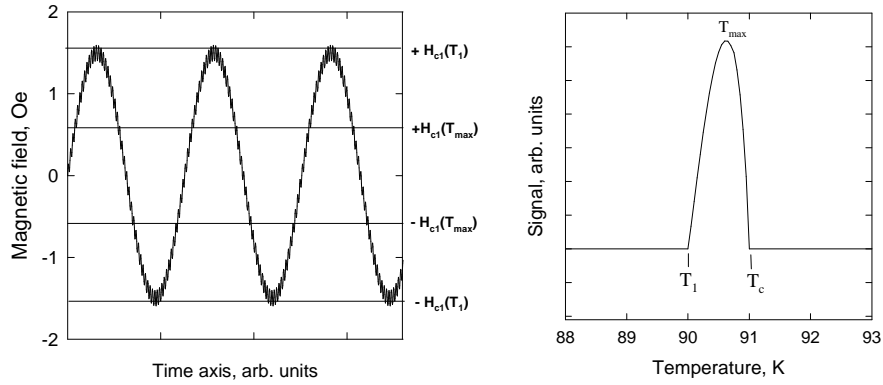


Fig. 4. – Left panel: schematic presentation of magnetic field variation with time near the sample. The low frequency component at frequency  $f$  is used to “virtually” remove the sample from the cell: when the amplitude of the low-frequency magnetic field  $H_0$  exceeds the first critical field  $H_{c1}$ , the magnetic field penetrates the sample volume. Right panel: signal at frequency  $2f$  extracted from the amplitude of the high-frequency signal. At  $T > T_c$  the signal disappears because the magnetic field penetrates the sample volume at all times; thus there is no variation of high-frequency signal amplitude with time. When  $T < T_1$ , signal also vanishes for an ideal superconductor ( $T_1$  is determined by the condition  $H_{c1}(T_1) = H_0$ ), because then  $H_{c1} > H_0$  and magnetic field is excluded at all times from the sample volume, and there is no variation of the of high-frequency signal amplitude with time. When  $T_1 < T < T_c$ , the magnetic field enters the sample volume twice per period of the low-frequency magnetic field  $T$  (frequency  $f = 1/T$ ), thereby producing amplitude modulation of the high-frequency signal with period  $T/2$  (at frequency  $2f$ ).

ter of detection coils. Using experimental parameters  $f=60$  KHz,  $n=300$ ,  $D=3.5$  mm,  $V_s=10^{-14}$  m<sup>3</sup> (sample size  $33 \times 33 \times 10$   $\mu\text{m}^3$ ),  $B=3 \cdot 10^{-5}$  T, and assuming that  $\chi=-1$  for  $T < T_c$ , we obtain  $\varepsilon=12$  nV. This estimate is fairly close to experimental values. Eq.1 is also helpful in estimating ways of increasing the sensitivity of the experimental setup. It is evident that when parameters  $n$ ,  $D$ ,  $B$  are optimized, one can increase the exciting frequency  $f$  in order to increase the sensitivity. However, increasing the operating frequency introduces problems related to the fact that stray capacitances of all electrical leads and cables become important. The details of the setup are described elsewhere [18].

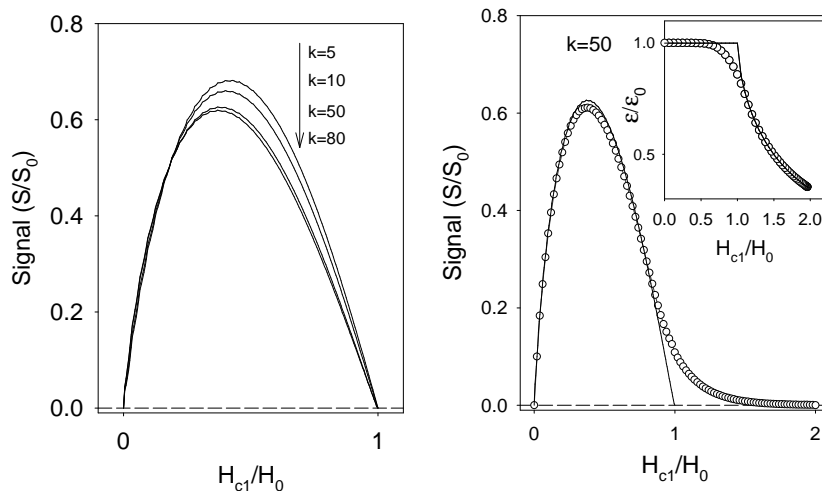


Fig. 5. – Signal dependence for type II superconductors calculated for different values of the Ginzburg-Landau parameter  $k$ , using Hao-Clemm theory (see text). Right panel illustrates how the signal shape is modified if the sharp cusp in the magnetization curve at  $H_{c1}$  is smeared out by experimental conditions (e.g., when the amplitude of the high-frequency magnetic field is not negligible compared to the amplitude of the low-frequency field) or by irreversibility effects in magnetization.

In Fig. 2 the schematic representation of the setup is given; we refer the reader to Refs. [13, 17, 18] for details. We will give below representative examples of  $T_c$  measurements at megabar pressures.

**3.4. Background issues.** – Samples of 99.9995% purity S were loaded in Mao-Bell cells [24] made from Be-Cu and modified for measurements down to liquid helium temperatures. The gaskets made from nonmagnetic Ni-Cr alloy were used together with tungsten inserts to confine the sample; no pressure transmitting media were used. The gasket and insert may be responsible for the temperature dependent background seen in the raw temperature scans (e.g., Fig. 7a). Two peaks are clearly seen at  $\sim 10$ -12 K and  $\sim 17$  K. The second broad peak at lower temperatures arises from the sample outside of the flat culet, where pressure is considerably lower than within the center of the culet. The splitting of the 17 K peak is artificial and only reflects the fact that the signal amplitude has increased substantially with respect to the background.

The background signal in our measurements appeared to be ferro- or paramagnetic, as its phase is approximately opposite to that of the signal from the sample (diamagnetic) (see Fig. 7a). Because the background signal changes smoothly with temperature, we

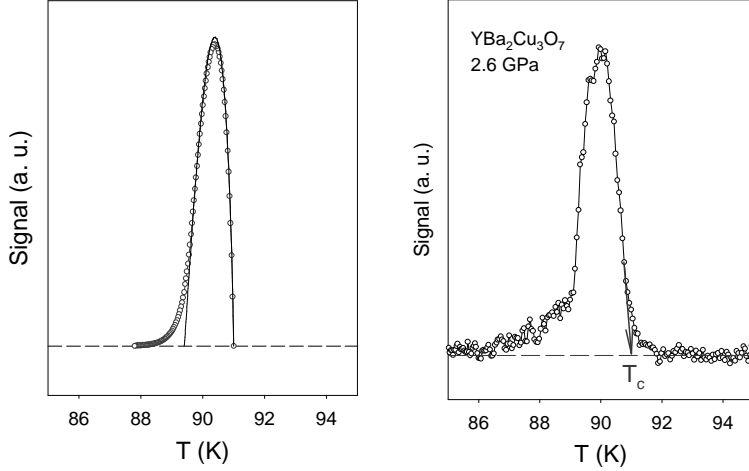


Fig. 6. – Comparison of the theoretical signal shape from Fig. 5 (right panel) with experimentally observed signal shape for slightly overdoped  $\text{YBa}_2\text{Cu}_3\text{O}_{7-x}$  in a He pressure medium.

can separate the signal from the background by the simple procedure illustrated in Fig. 7. We measure amplitude and phase of a sum of signal and background with a lock-in technique. The signal changes very abruptly in the vicinity of the superconducting transition, allowing us to see these changes both in amplitude and phase of the signal (Fig. 7a). It is straightforward to interpolate the background in the range of the superconducting transition with a smooth polynomial function. The total signal can be represented as the complex variable  $\mathbf{U} = A_S e^{i\phi_S}$ , and the interpolated background as  $\mathbf{B} = A_B e^{i\phi_B}$ ; our signal is then  $\mathbf{S} = A_S e^{i\phi_S} = \mathbf{U} - \mathbf{B}$  (the difference of two complex variables). The signal with background subtracted is shown in Fig. 7b, which clearly separates into the main sharp peak corresponding to the sample confined in the gasket hole with  $T_c \sim 16$  K, and a broad peak at lower temperatures that is due to the sample part which has flowed out of the gasket hole and is confined between the diamond culet and the gasket.

#### 4. – Simple Metals

We will focus in this section on simple  $s - p$  metals. Theoretically these metals are considered well understood. The first treatment of simple metals using pseudopotentials was given by McMillan [25]. This treatment was extended later by Allen and Cohen [26]. By definition, “simple metals” are metals in which outer ( $s$  and  $p$ ) conduction electrons are removed far enough in energy from  $d$  or  $f$  levels that these conduction electrons can be treated as nonlocalized nearly free electrons. In these metals the electron-ion interaction



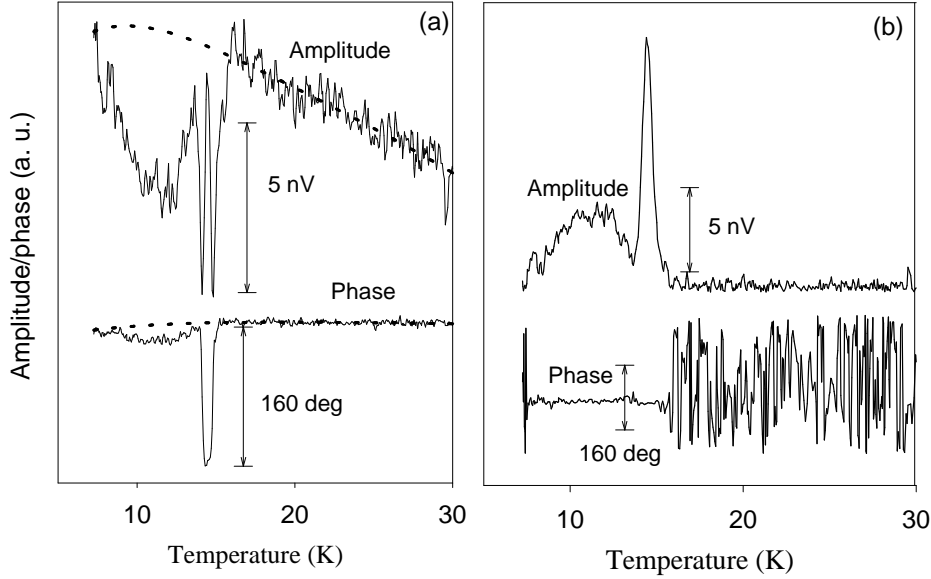


Fig. 7. – Superconducting signal from sulfur sample at 231 GPa, overlapped with the background. This figure illustrates how smooth background can be subtracted from the signal, using information for both signal amplitude and phase. See text for details.

can be treated using a pseudopotential approach, and the pseudowave functions are similar to the free-electron plane waves. In the following discussion we will use the Allen-Dynes [27] modified McMillan's [25] expression for  $T_c$  :

$$(2) \quad T_c = \frac{\omega_{log}}{1.2} \exp\left(\frac{-1.04(1+\lambda)}{\lambda - \mu^*(1+0.62\lambda)}\right).$$

Here the electron-phonon coupling constant is given by

$$(3) \quad \lambda = 2 \int \frac{d\omega \alpha^2(\omega) F(\omega)}{\omega} = \frac{N(\varepsilon_F) \langle I^2 \rangle}{M \langle \omega^2 \rangle},$$

where  $\alpha(\omega)$  is an average of the electron-phonon interaction,  $F(\omega)$  is the phonon density of states,  $N(\varepsilon_F)$  is the density of electron states at the Fermi level,  $\langle I^2 \rangle$  is the square of the electron-phonon interaction matrix element averaged over the Fermi surface,  $M$  is the atomic mass,  $\mu^*$  is Morel-Anderson effective Coulomb repulsion pseudopotential [28], and  $\omega_{log}$  and  $\langle \omega^2 \rangle$  are averages over the phonon spectrum given by [27]

$$(4) \quad \omega_{log} = \exp\left(\frac{2}{\lambda} \int_0^\infty \frac{d\omega}{\omega} \alpha^2 F(\omega) \ln \omega\right),$$

$$(5) \quad \langle \omega^2 \rangle = \frac{2}{\lambda} \int_0^\infty d\omega \alpha^2 F(\omega) \omega.$$

These expressions follow from a thorough analysis of the dependence of the superconducting transition temperature on material properties ( $\lambda$ ,  $\mu^*$ , phonon spectrum) as contained in Eliashberg theory [25, 27].

Within the pseudopotential model, McMillan [25] has derived the expression

$$(6) \quad \langle I^2 \rangle = \frac{8}{9} k_F^2 E_F^2 \langle v_q^2 \rangle,$$

where  $E_F$  and  $k_F$  are the Fermi energy and wavenumber, and  $\langle v_q^2 \rangle$  is a dimensionless average of the pseudopotential  $V(q)$  squared

$$(7) \quad \langle v_q^2 \rangle = \int_0^{k_F} V(q)^2 q^3 dq / \int_0^{k_F} V(0)^2 q^3 dq$$

For a free-electron gas, the density of states of one spin per atom is  $N(0) = 3Z/4E_F$  [25] ( $Z$  is the valence of the atom). Expressing the average phonon frequency in units of the ionic plasma frequency

$$(8) \quad \Omega_p^2 = 4\pi N Z^2 e^2 / M,$$

McMillan [25] gives the expression for the coupling constant as

$$(9) \quad \lambda = \frac{N(0) \langle I^2 \rangle}{M \langle \omega^2 \rangle} = \frac{1}{2} \pi \frac{E_F}{k_F e^2} \frac{\langle v_q^2 \rangle}{\langle \omega^2 \rangle / \Omega_p^2}.$$

The factor  $E_F/k_F e^2$  is just  $0.96/r_s$ , where  $r_s$  is the radius in atomic units of a sphere containing one electron; thus, a simple expression can be derived [25]

$$(10) \quad \lambda = \frac{1.51}{r_s} \frac{\langle v_q^2 \rangle}{\langle \omega^2 \rangle / \Omega_p^2}.$$

McMillan [25] noted that the observed phonon frequencies are extremely sensitive to small changes in pseudopotential and the important dependence of the coupling constant  $\lambda$  upon the pseudopotential arises from the  $\langle \omega^2 \rangle$  term in the denominator of Eq.10, rather than from the  $\langle v_q^2 \rangle$  in the numerator. Thus, for simple metals the pseudopotential theory predicts that the coupling constant varies inversely with the phonon frequency squared  $\lambda \cong C/(\langle \omega^2 \rangle / \Omega_p^2)$ . Making further approximations, McMillan arrives at his famous relation for simple metals:

$$(11) \quad \lambda \approx C' / M \langle \omega^2 \rangle.$$

Allen and Cohen [26] pointed out that in the jellium model

$$(12) \quad \langle \omega^2 \rangle / \Omega_p^2 \approx \frac{1}{2} q_D / k_s = (1/8 r_s) (3\pi^2 / Z)^{2/3}.$$

The potential strength  $\langle v_q^2 \rangle$  is a simple function of  $r_s$  in the jellium model, approximated by  $0.075 r_s$  in the region  $2 < r_s < 5$  (Fig. 4 in Ref. [26]). The net result of the jellium model analysis is that  $\lambda$  should scale as  $r_s Z^{2/3}$  on theoretical grounds, or as  $r_s Z^{5/3}$  empirically. We will use these results in our examination of the  $T_c$  trends in chalcogen family given below. For the analysis of high pressure data it is convenient to write down an explicit expression for the Hopfield parameter  $h = N(0) \langle I^2 \rangle$  as follows from pseudopotential relation for  $\langle I^2 \rangle$  from Eq.6

$$(13) \quad h = N(0) \langle I^2 \rangle = \frac{3Z}{4E_F} \langle I^2 \rangle = \frac{2}{3} Z k_F^2 E_F \langle v_q^2 \rangle.$$

Using  $\langle v_q^2 \rangle \sim r_s$ , and  $k_F^2 E_F \sim 1/r_s^4$ , we find that  $h \sim 1/r_s^3 \sim 1/V$ , which is widely used by experimentalists as an empirical relation for the Hopfield parameter in simple metals. In the next sections we will explore how these simple principles can be applied to real materials under pressure.

It should be noted, however, that real metals deviate from this simple model in many respects. As Allen and Cohen [26] have pointed out, there are considerable complications due to the following factors in real materials: (i) The actual Fermi surface is distorted away from a sphere near zone boundaries. (ii) The actual matrix elements deviate from the free-electron matrix elements near zone boundaries (iii) The phonon frequencies are anisotropic. We may add to this list: (iv) The effects of anharmonicity play substantial role in modifying electron-phonon interaction (MgB<sub>2</sub>, BaBiO<sub>3</sub>, High- $T_c$  superconductors) (v) Different electron energy bands (surfaces) have different contributions to electron-phonon coupling in materials with anisotropic energy bands (MgB<sub>2</sub>).

## 5. – Chalcogens: Sulfur, Selenium, Tellurium

We begin this section with estimates of scaling relations for pressure as follows from chemical considerations. From the virial theorem we have estimates for the total energy of valence electrons in the form [33]

$$(14) \quad W = \overline{T} + \overline{V} = -\frac{Z^2 e^2}{2a_0 n^2}$$

Here  $\overline{T}$  is averaged kinetic energy, and  $\overline{V}$  is averaged potential energy,  $Z$  is the number of valence electrons,  $e$  is electron charge,  $a_0$  is Bohr radius, and  $n$  is principal quantum number for the valence electrons ( $n=3$  for S,  $n=4$  for Se,  $n=5$  for Te). According to Pauling [33],

$$(15) \quad W = -\frac{e^2 a_0}{2n^2 r^2},$$

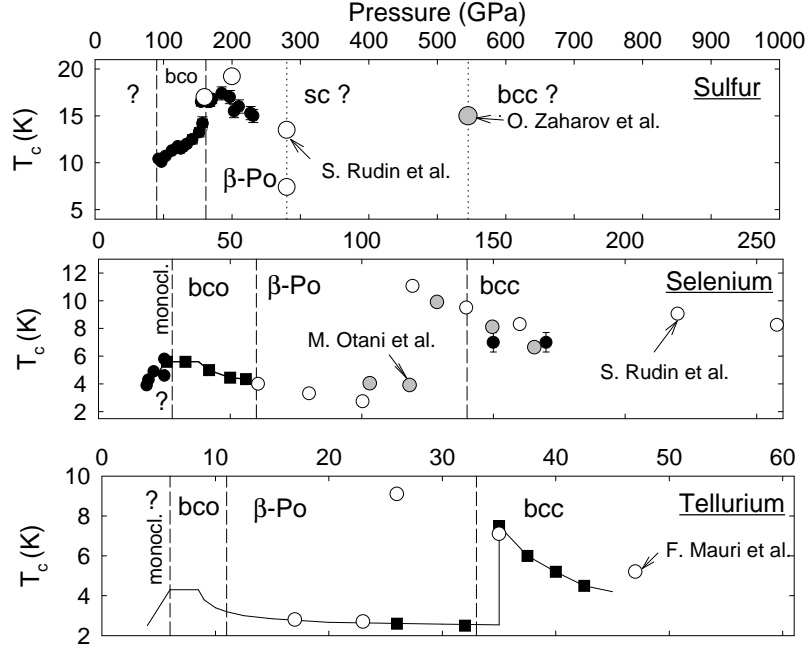


Fig. 8. – Superconducting  $T_c$  in S, Se, and Te. Data for S and Se below 25 GPa, and above 150 GPa are from Refs. [37, 8]. Data for Te and the remaining data for Se are from Refs. [34, 35, 32]. The observed similarity in  $T_c(P)$  curves illustrates the scaling relations derived in the text. Theoretical calculations are also shown (see Table II).

where  $r \sim a_0$  is average electronic radius of the valence orbitals. On the other hand, in the free-electron gas approximation, the total energy of the free-electron gas is given by the expression

$$(16) \quad E_F = (3\pi^2)^{2/3}(\hbar^2/2m)(Z/V_a)^{2/3},$$

where  $V_a$  is atomic volume,  $(4/3)Z\pi r_s^3 = V_a$ , and  $r_s$  is the radius of the sphere enclosing one electron. Assuming that in metallic state the total energy  $W \sim E_F$ , we find that  $n^2 r^2 \sim V_a^{2/3}$ , and thus  $W \sim 1/(n^2 V^{2/3})$ , where  $V$  is the total volume. By noting that  $P \sim \frac{\delta W}{\delta V}$  we obtain  $P \sim 1/(n^2 r^5)$ , ensuring the relation

$$(17) \quad n^2 r^5 P = \text{const}$$

TABLE I. – *Scaling relations for chalcogen family. Atomic volumes at phase transitions  $bcc \mapsto \beta$ -Po ( $V_{\beta-Po}$ ) are from Refs. [32, 31], atomic volumes at phase transitions  $\beta$ -Po  $\mapsto bcc$  ( $V_{bcc}$ ) are from Refs. [32, 39], pressure of the  $\beta$ -Po  $\mapsto bcc$  phase transition for sulfur is taken from theory [39]*

Element (n)	Te (5)	Se (4)	S (3)
$V_{\beta-Po}$ ( $\text{\AA}^3$ )	25.8	14.3	8.5
$r_v = r_s Z^{1/3}$ ( $\text{\AA}$ )	1.83	1.51	1.27
$P$ (GPa)	10.5	60	160
$n^2 r_v^5 P$ ( $\text{\AA}^5 \cdot \text{GPa}$ )	$5.4 \cdot 10^3$	$7.5 \cdot 10^3$	$4.7 \cdot 10^3$
$V_{bcc}$ ( $\text{\AA}^3$ )	21	11.3	7.4
$r_s Z^{1/3}$ ( $\text{\AA}$ )	1.71	1.39	1.21
$P$ (GPa)	33	140	545
$n^2 r_v^5 P$ ( $\text{\AA}^5 \cdot \text{GPa}$ )	$1.2 \cdot 10^4$	$1.2 \cdot 10^4$	$1.3 \cdot 10^4$

holds through the chalcogen series for equivalent free-electron-like metallic states as long as there is no substantial contribution from s- or d-orbitals to the energy balance. We have estimated that the product in Eq. 17 is indeed almost invariant for phase transition pressures in the chalcogen series from bcc to  $\beta$ -Po and from  $\beta$ -Po to bcc in metallic phases (illustrated by data in Table I). We also show the behavior of the superconducting  $T_c$  for S, Se, and Te in Fig. 8 by adjusting the pressure scale to the bcc phase transition pressure point. The observed similarities in  $T_c(P)$  mimic similarities in the phase transition sequence. Note also that theoretically predicted  $T_c$ 's for the  $\beta$ -Po and bcc phases are in good agreement with experiment. Table II shows theoretical estimates for averaged phonon frequencies and electron-phonon coupling  $\lambda$  as follows from theoretical calculations. It is remarkable that the  $\lambda$  values change very little when going from Te

TABLE II. – *Average phonon frequencies and electron-phonon coupling in the chalcogen family superconductors at selected pressures from theoretical work [39, 40, 41, 42]*

P (GPa)	$\omega_2$ ( $\text{cm}^{-1}$ )	$\omega_{log}$ ( $\text{cm}^{-1}$ )	$\lambda$	$T_c$ (K)	Ref.
Sulfur					
160 ( $\beta$ -Po)	375	305	0.76	17	[40]
280 ( $\beta$ -Po)	463	343	0.66	13.5	[40]
280 (sc)	481	389	0.53	7.4	[40]
584 (bcc)	411	422	0.58	15	[39]
Selenium					
103 ( $\beta$ -Po)	217	174	0.58	4.04	[42]
118( $\beta$ -Po)	227	179	0.57	3.91	[42]
129 (bcc)	204	157	0.83	9.9	[42]
166 (bcc)	234	185	0.66	6.6	[42]
Tellurium					
17 ( $\beta$ -Po)	109	57	0.8	2.8	[41]
23 ( $\beta$ -Po)	116	55	0.8	2.7	[41]
26 (bcc)	103	87	1.64	9.1	[41]
47 (bcc)	131	58	0.93	5.2	[41]

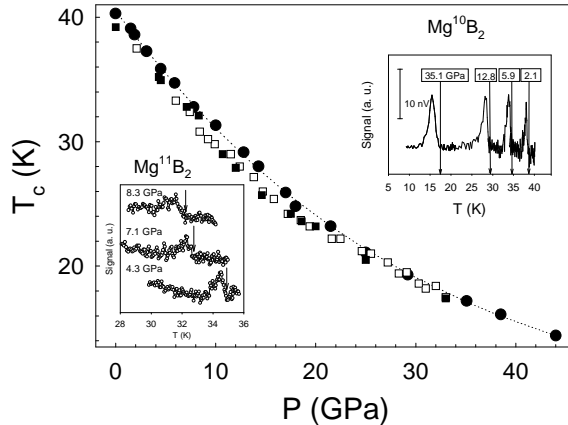


Fig. 9. – This figure shows pressure dependence of  $T_c$  in isotopically pure  $\text{MgB}_2$  samples, measured in He pressure medium. Corresponding insets show experimental temperature scans. Circles are used for  $\text{Mg}^{10}\text{B}_2$ , squares for  $\text{Mg}^{11}\text{B}_2$ ; full symbols are for compression and open symbols for decompression.

to S (except for the very high  $\lambda$  in Te bcc phase close to the phase transition, which is attributed to soft phonon modes [41]). Thus, instead of  $\lambda \sim r_s$  as we would expect from pseudopotential theory (see Ref. [26], and discussion after Eq. 12 in section 3), we have instead  $\lambda \sim \text{const}$ . If this trend continues to oxygen, we may expect rather high  $T_c$  values in atomic oxygen at pressures above 1000 GPa [43].

## 6. – $\text{MgB}_2$ and Phonon-Assisted Electronic Topological Transition

The recently discovered high-temperature superconductor  $\text{MgB}_2$  [44] has attracted considerable interest. Experiment [45, 46] as well as theory [47, 48, 49, 50] indicates that  $\text{MgB}_2$  can be treated as a phonon mediated superconductor. Calculations show that the strongest coupling is realized for the phonon branch in the Brillouin zone from  $\Gamma$  ( $E_{2g}$  phonon) to  $A$  ( $E_{2u}$  phonon), which is related to vibrations of the B atoms [48, 49, 50]. This makes  $\text{MgB}_2$  a unique system in which a single phonon branch appears to dominate the superconducting properties within the framework of a phonon-mediated mechanism for superconductivity. By knowing the pressure dependence of these phonon frequencies and the pressure dependence of  $T_c$ , the electron-phonon coupling in this material can be directly addressed.

We measured  $T_c(P)$  in isotopically pure samples of  $\text{MgB}_2$  (samples were similar to those used in Ref.[45]), with  $^{10}\text{B}$  and  $^{11}\text{B}$ . The details of the experiment are presented in Ref. [9]. In Fig.9 we show the  $T_c$  as a function of pressure; temperature scans at selected pressures are also shown. The signal observed is close to the limit of the sensitivity of our setup. The signal is superimposed on the nonlinear paramagnetic background from the gasket material at lower temperatures (below 25 K), which has a characteristic  $\frac{1}{T}$

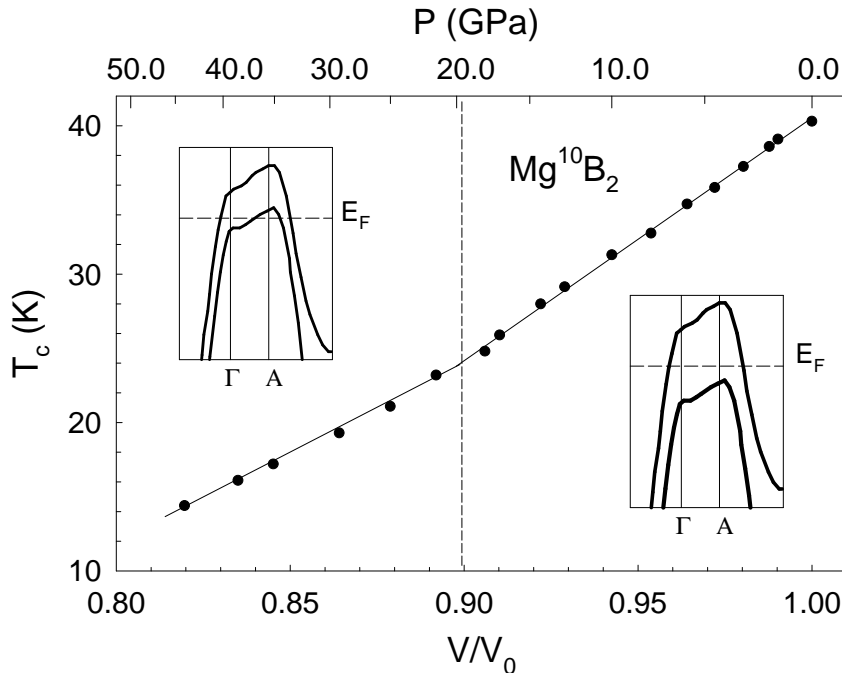


Fig. 10. – Superconducting critical temperature ( $T_c$ ) plotted as a function of volume is linear, with kink at about 20 GPa for  $\text{Mg}^{10}\text{B}_2$ , respectively. Insets illustrate the proposed phonon-assisted electronic topological transition, responsible for the observed effect. See text for details.

dependence (subtracted from the data for  $\text{Mg}^{10}\text{B}_2$ ). However, the onset of  $T_c$  can be reliably identified with an accuracy 0.2-0.8 K (depending on the actual quality of the data, as illustrated in Fig.9) up to the highest pressures reached in this experiment.

We plot  $T_c$  for  $\text{Mg}^{10}\text{B}_2$  as a function of volume in Fig.10. One can clearly distinguish a kink in  $T_c(V)$  at a volume that corresponds to 20 GPa. We observe a similar kink at 15 GPa for  $\text{Mg}^{11}\text{B}_2$  [9]. Pressure dependence of the  $E_{2g}$  phonon was measured recently in our laboratory [51]. We have measured  $E_{2g}$  Raman mode frequency in  $\text{Mg}^{10}\text{B}_2$  at room temperature to 50 GPa [9] to understand the anomaly in  $T_c$ ; we observed similar anomaly in the pressure dependence of the Raman mode slightly above 20 GPa. The details of the Raman experiment are published elsewhere [52].

At lower pressures the zero-point motion of the boron atoms for the  $E_{2g}$  mode strongly splits the boron in-plane  $\sigma$  bands, so that the lower band moves below the Fermi level, thereby crossing it and fulfilling the condition for an Electronic Topological Transition (ETT) (Fig. 10, right inset). This means that for a frozen-phonon calculation there should be an anomalous contribution to the total energy, that behaves similarly to  $2\frac{1}{2}$  power term in the free energy, suggested by Lifshitz [53], with the amplitude of the phonon mode being a parameter that drives the electronic subsystem through the transition. As such, the phonon frequency is strongly anharmonic, and its volume derivative (the Grüneisen parameter) may even diverge at the transition. At higher pressures the zero-point motion does not split the  $\sigma$  band strongly enough for the lower band to cross the

Fermi level (Fig. 10, left inset). Thus, the system is always at conditions in which there is no anomalous contribution to the free energy from ETT-like  $2\frac{1}{2}$  power terms, and the phonon mode and  $T_c$  behave in a more regular manner. Between those two regimes there should be a small pressure range in which the amplitude of the zero-point motion is just enough for the top of the lower band to coincide with the Fermi level. It is proposed that this condition is almost fulfilled at the observed kinks in pressure dependencies of  $T_c$  and  $E_{2g}$  phonon frequency.

The lower pressure for the observed transition in  $\text{Mg}^{11}\text{B}_2$  versus  $\text{Mg}^{10}\text{B}_2$  [9] may be due to the isotope effect: the zero-point motion for a heavier atom is smaller, and the matching condition for the  $\sigma$  band is fulfilled at lower compression of the lattice. Several arguments support the observed isotope trend, following the reasoning proposed by An and Pickett [48]. They noticed that the  $\sigma$  bands belonging to B, which form cylindrical Fermi surface sheets [47], can be treated as quasi-two-dimensional. The states in these bands contribute most of the electron-phonon coupling responsible for superconductivity [48]. The overall splitting of the  $\sigma$  band is characterized by  $p-p$  matrix element  $t_{pp\sigma} \sim d^{-3}$ , where  $d$  is B-B bond length. Thus, the deformation potential of the  $\sigma$  band will be proportional to the derivative of the above matrix element with respect to  $d$  ( $E_{2g}$  mode modulates B-B distance), and thus  $|\tilde{D}| \sim d^{-4}$ . We have determined earlier that the phonon frequency of the  $E_{2g}$  mode scales as  $\omega \sim (a/a_0)^{-10.8} = (d/d_0)^{-10.8}$  below 15 GPa [51]. The amplitude of the zero-point motion  $u \sim \omega^{-1/2} \sim (d/d_0)^{5.4}$ , which means that the splitting of  $\sigma$  bands  $\Delta E \sim \tilde{D}u \sim (d/d_0)^{1.4}$  decreases almost proportionally with the B-B bond length.

The low-pressure regime for both isotopic compounds suggests a strong contribution from ETT anomalies to the observed properties of the materials. It should be noted that the electron-phonon coupling may be strongly affected by the non-adiabatic effects due to the violation of the condition that the Debye frequency is much less than the Fermi energy  $\omega_D/E_F \ll 1$  [54] close to the ETT regime. We also expect large effects of uniaxial stresses and stoichiometry on the pressure dependence of the superconducting transition in  $\text{MgB}_2$ .

## 7. – Conclusions

Developments in magnetic susceptibility techniques for diamond anvil cell applications have been reviewed here with an in-depth discussion of the basics of the recently improved double modulation technique. The method has been applied to studies above 230 GPa without a pressure medium and above 40 GPa with He pressure medium. The pressure-limiting factors have not been yet explored in detail, and high-pressure limit of the technique remains to be established. Numerical estimates/extrapolations indicate that superconductivity measurements on samples down to 10  $\mu\text{m}$  in diameter are within reach [18].

We have measured superconductivity in S over broad pressure range from metalization onset at 90 GPa (bco phase) to 231 GPa into the  $\beta$ -Po phase. Superconductivity in Se was studied below 33 GPa, and the pressure-induced increase of  $T_c$  was discovered in a yet to be identified low-pressure phase; we also observed  $T_c \sim 7.5$  K above 160 GPa. These experiments, together with previous pressure studies of superconductivity in Te and Se, indicate that pressure-induced changes of  $T_c$  in the chalcogens follow a scaling relation  $n^2 r_s^5 P \approx \text{const.}$  (Eq. 17). The electron-phonon coupling constant in the chalcogens in the corresponding phases appear to be remarkably similar, a result that can not be explained



by the trends derived from simple pseudopotential model.

MgB<sub>2</sub> is an example of a less isotropic simple s-p metal, with a T<sub>c</sub> value almost at the limit of what is expected from a phonon-mediated superconductor. We have explored the pressure dependence of T<sub>c</sub> for two B isotopes: Mg<sup>10</sup>B<sub>2</sub> and Mg<sup>11</sup>B<sub>2</sub>. Combining T<sub>c</sub> studies with Raman measurements of the E<sub>2g</sub> mode, we were able to find a correlation between the highly anharmonic behavior of the phonon and T<sub>c</sub>(P) anomaly in Mg<sup>11</sup>B<sub>2</sub>. A Lifshitz ETT [53], with the amplitude of the zero point motion of the B atoms taken into account [9], can explain the origin of these effects.

\* \* \*

This work was supported by the National Science Foundation, the Department of Energy, the Center for High Pressure Research (CHiPR). Special thanks are to the former Director of the Geophysical Laboratory Charles Prewitt, who endorsed and supported this work under the auspices of CHiPR.

#### REFERENCES

- [1] HEMLEY R. J. and ASHCROFT N. W., *Physics Today*, **51** (1998) 26.
- [2] HEMLEY R. J. and MAO H. K., *Encyclopedia of Applied Physics*, ed. G. L. Trigg, VCH Publishers, New York, **18** (1997) 555.
- [3] GAO L. ET AL., *Phys. Rev. B.*, **50** (1994) 4260.
- [4] BARDEEN J., COOPER L. N. and SCHRIEFFER J. R., *Phys. Rev.*, **108** (1957) 1175.
- [5] ONNES KAMERLINGH. H., *Commun. Phys. Lab. Univ. Leiden*, **119b,120b,122b,124c** (1911) .
- [6] WU M. K. ET AL., *Phys. Rev. Lett.*, **58** (1987) 908.
- [7] CHU C. W. ET AL., *Phys. Rev. Lett.*, **58** (1987) 405.
- [8] GREGORYANZ E. A., STRUZHKN V. V., TIMOFEEV YU. A., HEMLEY R. J., and MAO H. K., *Phys. Rev. B.*, (2001) in press.
- [9] STRUZHKN V. V., GONCHAROV A. F., HEMLEY R. J., MAO H. K., LAPERTOT G., BUD'KO S. L., and CANFIELD P. C., *cond-mat/0106576*, (2001) .
- [10] EREMETS M. I., STRUZHKN V. V., TIMOFEEV YU. A., HEMLEY R. J., and MAO H. K., *Science*, **293** (2001) 272
- [11] KLOTZ S., SCHILLING J. S. and MÜLLER P., *Frontiers of High-Pressure Research*, edited by HOCHHEIMER H. D. and ETTERS R. D. (Plenum Press, Hew York) 1991, pp. 473-491.
- [12] TISSEN V. G., PONYATOVSKII E. G., NEFEDOVA M. V., PORSCH F., and HOLZAPFEL W. B., *Phys. Rev. B*, **53** (1996) 8238.
- [13] TIMOFEEV YU. A, *Prib. Tekh. Eksper. (in Russian)*, **5** (1992) 186.
- [14] RAPHAEL M. P., REEVES M. E. and SKELTON E. F., *Rev. Sci. Instrum*, **69** (1998) 1451.
- [15] ISHIZUKA M., AMAYA K. and ENDO S., *Rev. Sci. Instrum*, **66** (1995) 3307.
- [16] ISHIZUKA M., IKETANI M. and ENDO S., *Phys. Rev. B.*, **61** (2000) R3823
- [17] TIMOFEEV YU. A., MAO H. K., STRUZHKN V. V., and HEMLEY R. J., *Rev. Sci. Instrum*, **70** (1999) 4059.
- [18] TIMOFEEV YU. A., STRUZHKN V. V., GREGORYANZ E., MAO H. K., and HEMLEY R. J., *Rev. Sci. Instrum.*, (2001) in press.
- [19] AMAYA K., SHIMIZU K., EREMETS M. I., KOBAYASHI T. C., ENDO J., *Phys. C: Condens. Matter*, **10** (1998) 11179
- [20] HEMLEY R. J., EREMETS M. I., MAO H. K., *Frontiers of High-Pressure Research II: Application of High Pressure to Low Dimensional Novel Electronic Materials*, edited by H. D. HOCHHEIMER (Kluwer, Amsterdam) in press.
- [21] HAO Z., CLEMM J. R., McELFRESH M. W., CIVALE L., MALOZEMOFF A. P., and HOLTZBERG F., *Phys. Rev. B*, **43** (1991) 2844.

- [22] XU M., SOK Y., OSTENSON J. E., FINNEMORE D. K., and DABROWSKI B., *Phys. Rev. B*, **53** (1996) 15313.
- [23] SHATZ A., SHAULOV A., and YESHURUN Y, *Phys. Rev. B*, **48** (1993) 13871.
- [24] MAO H. K., HEMLEY R. G., and MAO A. L., in *High-Pressure Science and Technology*, edited by S. SCHMIDT ET AL. (American Institute of Physics, New York) 1994, pp. 1613-1616.
- [25] McMILLAN W. L., *Phys. Rev.*, **167** (1968) 331.
- [26] ALLEN P. B. and COHEN M. L., *Phys. Rev.*, **187** (1969) 525.
- [27] ALLEN P. B. and DYNES R. C., *Phys. Rev. B*, **12** (1975) 905.
- [28] MOREL P. and ANDERSON P. W., *Phys. Rev.*, **125** (1962) 1263.
- [29] PARTHASARATHY G. and HOLZAPFEL W. B., *Phys. Rev. B*, **37** (1988) 8499.
- [30] AKAHAMA Y., KOBAYASHI M. and KAWAMURA H., , **47** (1993) 20.
- [31] LUO H., DESGRENIERS S., VOHRA Y. K., and RUOFF A., , **71** (1993) 2943.
- [32] AKAHAMA Y., KOBAYASHI M., and KAWAMURA H., , **48** (1993) 6862.
- [33] Pauling L, *The Nature of the Chemical Bond and the Structure of Molecules and Crystals: an Introduction to Modern Structural Chemistry* (Ithaca, N. Y., Cornell University press)1991.
- [34] BERMAN I. V., BINZAROV Z. I., and ZHURKIN P., *Sov. Phys. Solid State*, **14** (1973) 2192.
- [35] BUNDY F. P. and DUNN K. J., *Phys. Rev. B*, **22** (1980) 3157.
- [36] AKAHAMA Y., KOBAYASHI M., and KAWAMURA H., *Solid State Commun.*, **84** (1992) 803.
- [37] STRUZHUKIN V. V., HEMLEY R. J., MAO H. K., and TIMOFEEV YU. A., *Nature*, **390** (1997) 382.
- [38] SHIMIZU K., SUHARA K., IKUMO M., EREMETS M. I., and AMAYA K., *Nature*, **393** (1998) 767.
- [39] ZAKHAROV O. and COHEN M. L., , **52** (1995) 12572.
- [40] BUNDY F. P. and LIU A., *Phys. Rev. Lett.*, **83** (1999) 3049.
- [41] MAURI F. *et al.*, *Phys. Rev. Lett.*, **77** (1996) 1151.
- [42] OTANI M. *et al.*, *Phys. Rev. B*, **63** (2001) 104516.
- [43] OTANI M., YAMAGUCHI K., MIYAGI H., and SUZUKI N. , *Rev. High Press. Sci. Tech.*, **7** (1998) 178.
- [44] NAGAMATSU J., NAKAGAWA N., MURANAKA T., ZENITANI Y., and AKIMITSU J.,, *Nature*, **410** (2001) 63.
- [45] BUD'KO S. L. *et al.*, *Phys. Rev. Lett.*, **86** (2001) 1877.
- [46] HINKS D. G., CLAUS H., and JORGENSEN J. D., *Phys. Rev. Lett.*, **86** (2001) 1877.
- [47] KORTUS J., MAZIN I. I., BELASHCHENKO K. D., ANTROPOV V. P., and L. L. BOYER, *Phys. Rev. Lett.*, **86** (2001) 4656.
- [48] AN J. M. and PICKETT W. E., *Phys. Rev. Lett.*, **86** (2001) 4366.
- [49] KONG Y., DOLGOV V., JEPSEN O., and ANDERSEN O. K., *Phys. Rev. B.*, **64** (2001) 0205011R.
- [50] YILDIRIM T *et al.*, *Phys. Rev. Lett.*, **87** (2001) 037001.
- [51] GONCHAROV A. F., STRUZHUKIN V. V., GREGORYANZ E., HU J., HEMLEY R. J., MAO H. K., LAPERTOT G., BUD'KO S. L., and CANFIELD P. C., *Phys. Rev. B*, **64** (2001) 100509(R).
- [52] GONCHAROV A. F. *et al.*, *see this volume*, (2001) .
- [53] LIFSHITZ I. M., *Sov. Phys. JETP*, **11** (1960) 1130.
- [54] MIGDAL A. B., *Sov. Phys. JETP*, **34** (1958) 996.